

Structural Flexibility of the N-terminal β -Barrel Domain of 15-Lipoxygenase-1 Probed by Small Angle X-ray Scattering. Functional Consequences for Activity Regulation and Membrane Binding

This paper is dedicated to Professor S. M. Rapoport, the discoverer of this enzyme, who passed away July 27th, 2004.

Michal Hammel^{1†}, Matthias Walther^{2†}, Ruth Prassl^{1*} and Hartmut Kuhn^{2*}

¹*Institute of Biophysics and X-Ray Structure Research of the Austrian Academy of Sciences Schmiedlstr. 6, A-8042 Graz Austria*

²*Institute of Biochemistry University Clinics Charité Humboldt University Monbijoustraße 2, 10117 Berlin Germany*

Mammalian lipoxygenases form a heterogeneous family of lipid peroxidizing enzymes, which have been implicated in synthesis of inflammatory mediators, in cell development and in the pathogenesis of various diseases (atherosclerosis, osteoporosis) with major health political importance. The crystal structures of two plant lipoxygenase isoforms have been solved and X-ray coordinates for an inhibitor complex of the rabbit 15-lipoxygenase-1 are also accessible. Here, we investigated the solution structure of the ligand-free rabbit 15-lipoxygenase-1 by small angle X-ray scattering. From the scattering profiles we modeled the solution structure of the enzyme using two independent *ab initio* approaches. Preliminary experiments indicated that at low protein concentrations (<1 mg/ml) and at 10 °C the enzyme is present as hydrated monomer. Superposition of the high resolution crystal structure and our low resolution model of the solution structure revealed two major differences. (i) Although the two models are almost perfectly superimposed in the region of the catalytic domain the solution structure is stretched out in the region of the N-terminal β -barrel domain and exhibits a bigger molecular volume. (ii) There is a central bending of the enzyme molecule in the solution structure, which does not show up in the crystal structure. Both structural peculiarities may be explained by a high degree of motional freedom of the N-terminal β -barrel domain in aqueous solutions. This interdomain movement may be of functional importance for regulation of the catalytic activity and membrane binding.

© 2004 Elsevier Ltd. All rights reserved.

Keywords: eicosanoids; inflammation; cell differentiation; structural flexibility; reaction mechanism

*Corresponding authors

Introduction

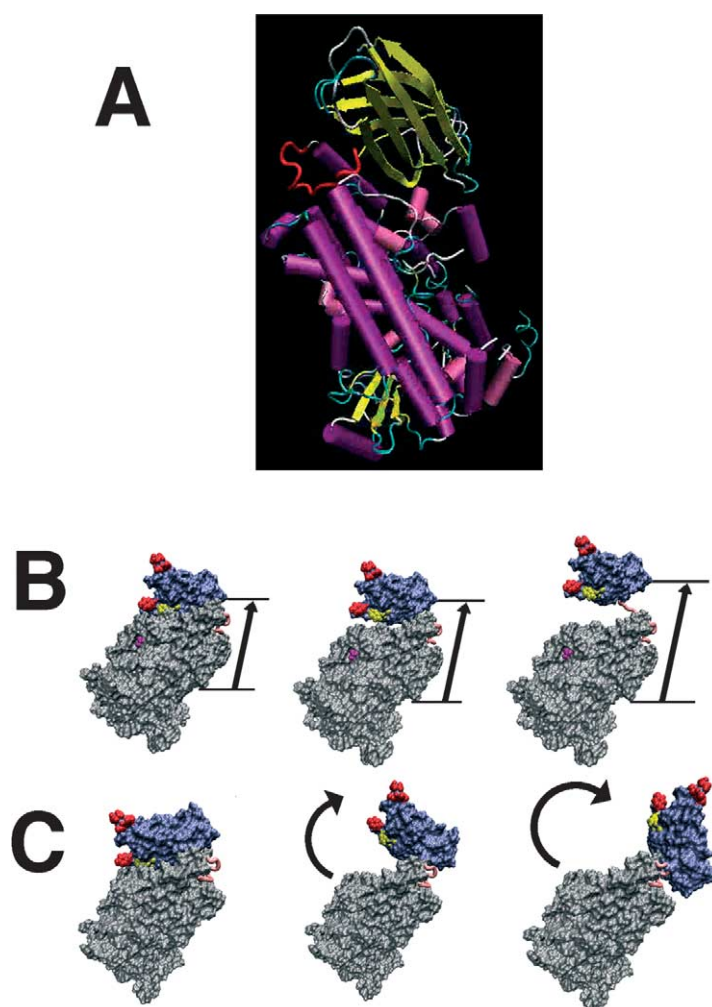
Lipoxygenases (LOXs) constitute a heterogeneous family of lipid peroxidizing enzymes that

catalyze dioxygenation of free and/or esterified polyunsaturated fatty acids to the corresponding hydroperoxy derivatives.¹ Mammalian LOXs have been implicated in the biosynthesis of inflammatory mediators, such as leukotrienes^{2,3} and lipoxins,⁴ but have also been suggested to be involved in cell differentiation,^{5,6} carcinogenesis⁷ and in the pathogenesis of atherosclerosis⁸ and osteoporosis.⁹ The crystal structures of two plant LOX isoforms (soybean LOX-1^{10,11} and -3¹²) and of a mammalian enzyme–inhibitor complex (rabbit 15-LOX-1¹³) have been reported and there are additional data sets available for various LOX–ligand complexes.^{14–16} Moreover, 3D models for the structure of the human

† M.H. & M.W. contributed equally to this paper.

Abbreviations used: SAXS, small angle X-ray scattering; LOX, lipoxygenase; 12S-HETE, 12-H(p)ETE, (12S,5Z,8Z,10E,14Z)-12-hydro(pero)xyeicosa-5,8,10,14-tetraenoic acid; 15S-HETE, 15-H(p)ETE, (15S,5Z,8Z,11Z,13E)-15-hydro(pero)xyeicosa-5,8,11,13-tetraenoic acid; SMP, sub-mitochondrial particles.

E-mail addresses of the corresponding authors: ruth.prassl@oeaw.ac.at; hartmut.kuehn@charite.de



Scheme 1. Two-domain structure of the rabbit 15-LOX-1 and possibilities of interdomain movement. (A) The crystal structure of the rabbit 15-LOX-1 is given as ribbon diagram and the random coil interconnecting the two domains is marked in red. To demonstrate possible interdomain movement (B and C) the surface structure of the enzyme was used. The major sequence determinants of membrane binding are given in red and Trp100 in yellow (see Figure 7). The domain-connecting random coil is indicated in pink. (B) Linear dislocation of the N-terminal domain (direction is given by the arrows), which leads to stretching of the overall enzyme shape and to a higher degree of solvent exposure of Trp100. The carboxylic group of arachidonic acid bound in the substrate-binding pocket is shown in violet. (C) Swing-out of the β -barrel domain relative to the catalytic subunit. Such movement (direction given by the arrow) induced stretching and bending of the enzyme molecule and also leads to solvent exposure of Trp100.

5-LOX have been worked out on the basis of the rabbit 15-LOX crystal structure and multiple amino acid alignments.¹⁷ Taken together, these data indicate a high degree of conservation of essential structural features in plant and animal LOXs. This conclusion is quite surprising if one considers that plant and animal LOXs only share a low degree of amino acid conservation and differ from each other with respect to essential protein-chemical and enzymatic properties.

All LOX isoforms consist of a single polypeptide chain that is folded into a two-domain structure.^{10–13} The large C-terminal catalytic domain of the rabbit 15-LOX-1 (molecular mass of 75 kDa) comprises about 550 amino acid residues and is largely helical.¹³ It contains the catalytic non-heme iron cluster, which is buried deeply inside the putative substrate-binding pocket.¹⁸ The small N-terminal domain that involves 110 amino acid residues

consists of two four-stranded antiparallel β -sheets, and shares a 1600 \AA^2 interface with the catalytic domain.¹³ Both domains are interconnected by an unstructured stretch of amino acids (random coil) that comprises amino acid residues 111 to 124 (Scheme 1(A)). This structural motif may allow significant interdomain movement. The soybean LOX-1, which is composed of 839 amino acid residues (96 kDa), does also fold into a two-domain structure.^{10,11} The two structural subunits share a 2600 \AA^2 contact plane and the interdomain interface constitutes a solvent-filled crevice.¹¹ These data suggest that the two domains are rather loosely interconnected and may exhibit a high degree of interdomain motional freedom. More detailed evaluation of the X-ray coordinates of the soybean LOX-1 (comparison of the *B*-value pattern) suggested that the overall structures of the two domains are rather stable but that the N-terminal

β -barrel domain may move as a unit relative to the catalytic subunit.¹¹ It was suggested that in the crystal structure the β -barrel domain may rock across the surface of the catalytic domain rather than swinging away from it. In aqueous solutions, where enzyme molecules are highly hydrated and where steric constraints for motional freedom may be reduced, the interdomain interaction may even be weaker leading to a higher degree of interdomain motional freedom. This motional flexibility may alter the overall shape of the LOX molecule in aqueous solutions.

Small angle X-ray scattering (SAXS) is an effective method to investigate the low-resolution structure of proteins at low concentrations in aqueous solutions.¹⁹ The overall shape and quaternary structure of proteins as determined by SAXS have been successfully applied to model low-resolution structures of proteins.^{20,21} Comparison between the theoretical scattering curve calculated from the crystal structure and the experimental scattering curves can be used to assign structural differences, which become apparent by superposition of the 3D reconstitution model with its atomic structure determined by X-ray crystallography.^{22,23}

For this study we measured small angle X-ray scattering of the rabbit reticulocyte 15-LOX at low concentrations in aqueous solution at near physiological pH. Low-resolution models of the 3D structure were restored from the SAXS profiles using two independent *ab initio* modeling approaches. Superimposition of the crystal and the solution structures of the enzyme revealed that the low-resolution model of the catalytic domain matches the crystal structure. In contrast, in the region of the N-terminal β -barrel domain we observed an obvious mismatch. These differences may be attributed to a more pronounced structural flexibility, in particular to a higher degree of motional freedom of the N-terminal β -barrel domain.

Results

15-LOX preparation and partial characterization of the enzyme

The native rabbit 15-LOX-1 was prepared from a stroma-free lysis supernatant (20,000g) of a reticulocyte-rich blood cell suspension by a three-step purification procedure²⁴ that included fractionated ammonium sulfate precipitation and consecutive hydrophobic interaction and anion exchange chromatography on a preparative Mono-Q-FPLC column. To determine the degree of purity of the final enzyme preparation and its molecular mass we performed analytical gel filtration and SDS-PAGE. In gel filtration (data not shown) we determined a molecular mass of about 80 kDa, which is consistent with a previous report.²⁵ In SDS-PAGE the molecular mass was about 75 kDa (data not shown) and the enzyme preparation exhibited a high degree of purity (>95%). For

further characterization of the enzyme preparation we investigated its reaction kinetics with arachidonic acid as substrate and the product specificity. In these experiments we observed a K_M value (arachidonic acid) of $8.1(\pm 1.0)$ μM and a V_{max} of $9.5(\pm 0.9)$ s^{-1} . The product specificity was checked by a combined reverse phase and chiral phase-HPLC strategy. The major reaction product was identified as 15S-H(p)ETE with 12S-H(p)ETE being formed in smaller quantities (15S-H(p)ETE/12S-H(p)ETE-ratio of 91 : 9). If required, the final enzyme preparations were concentrated using Ultrafree Biomax 30 K filters (Milipore, Bedford, MA) and stored at -80°C as aqueous solutions containing 10% (v/v) glycerol.

Protein aggregation determined by small angle X-ray scattering

In preliminary experiments performed on a Hecus SAXS camera (see Material and Methods) the long-time stability of the LOX solution was examined. The sample incubated at 20°C was measured four times under identical conditions

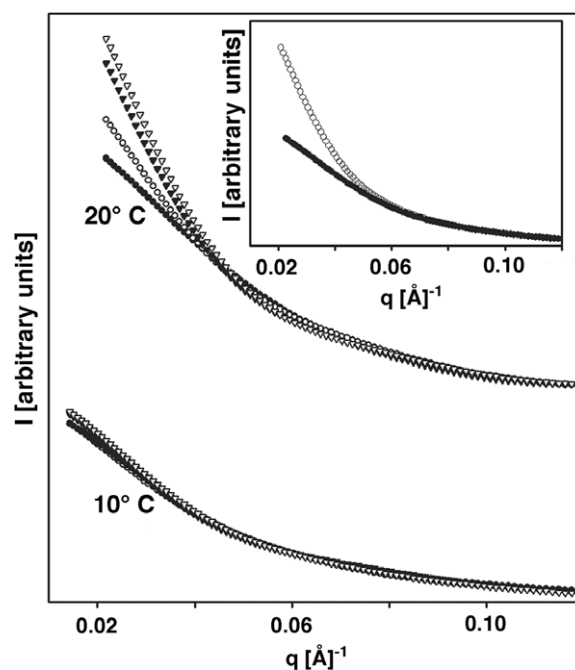


Figure 1. Desmeared experimental SAXS profiles of the rabbit 15-LOX-1. The rabbit 15-LOX-1 was prepared as described in Materials and Methods and small angle X-ray scattering was measured with a Hecus SAXS camera at 20°C (top) and 10°C (bottom). Filled circles, initial time point; open circles, after six hours; filled triangles, after 12 hours; open triangles, after 18 hours. The maximal exposure time of the protein sample to the X-ray beam was two hours and a protein concentration 0.7 mg/ml was adjusted. Due to the low signal-to-noise ratio for low protein concentrations at higher q -values only a small q -range (0.01 \AA^{-1} to 0.12 \AA^{-1}) could be used for further calculations. Inset: SAXS profiles for protein concentrations of $c = 0.7$ mg/ml (filled circles) and $c = 5.0$ mg/ml (open circles). The protein concentrations were normalized to unity.

within a time period of 18 hours. The significant increase in scattering intensity at low angles ($q < 0.04 \text{ \AA}^{-1}$) suggests protein aggregation. At higher angles ($q > 0.08 \text{ \AA}^{-1}$) X-ray scattering is less sensitive for inter-particle interaction and hence the scattering pattern remains unaltered (Figure 1, upper traces). In contrast, when the same experiment was carried out at 10°C the aggregation tendency was minimal and the scattering pattern did not change even during long-term incubations (Figure 1 lower traces). To test whether or not the protein concentration may impact the aggregation behavior comparable measurements were performed at two different protein concentrations. The desmeared experimental SAXS profiles of 15-LOX at 0.7 mg/ml and 5 mg/ml (10°C) are shown in Figure 1 (inset). Here again, the high intensity signals at low scattering angles ($q < 0.04 \text{ \AA}^{-1}$) observed for the concentrated protein solution indicate a tendency of protein aggregation. The scattering patterns at higher angles ($q > 0.08 \text{ \AA}^{-1}$) were similar for both protein concentrations, suggesting that there were no concentration-dependent alterations in the overall conformation of the LOX molecule. Similar experiments were carried out several times with three different enzyme preparations and the results were always comparable.

Synchrotron SAXS experiments

From the results of the preliminary experiments it was concluded that temperature, protein concentration and duration of the measuring period are critical for SAXS measurements on 15-LOX-1. Since reliable conclusions can only be drawn from SAXS profiles of non-aggregated monomeric protein solutions the final experiments were carried out at 10°C and at LOX concentrations $< 1 \text{ mg/ml}$. Moreover, we shortened the time span of measurements as much as possible and used a high-brilliance synchrotron beamline as X-ray source. Two sets of data have been collected with two different enzyme preparations and very similar results were always obtained. In Figure 2 a typical scattering profile of the rabbit 15-LOX-1 is shown. The radius of gyration ($R_G = 33.4 (\pm 0.5) \text{ \AA}$) was estimated from the Guinier plot (Figure 2, inset). The scattered intensities follow closely the Guinier law in the low q -range, indicating a non-aggregated state of the protein solution. The R_G value extracted from the scattering data was in good agreement with that derived from the $P(r)$ function $R_G = 34.0 (\pm 0.2) \text{ \AA}$. A molecular mass for the hydrated 15-LOX-1 of about 83 kDa was determined. This value is somewhat higher than the theoretical value calculated from the amino acid composition (75 kDa) and that obtained experimentally from SDS-PAGE. However, it was more similar to the value determined by gel filtration (see above). This finding is in line with previous observations suggesting that non-globular proteins may exhibit a higher molecular mass in aqueous solutions.^{26,27} Similar differences were also observed for the

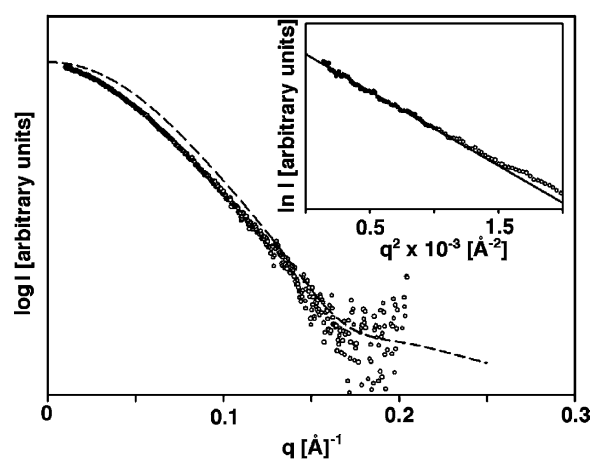


Figure 2. Comparison of the experimental SAXS profile of the rabbit 15-LOX and theoretical scattering profile calculated from the crystal structure. Experimental data are indicated by the open circles and the theoretical SAXS profile calculated from the crystal structure is given by the broken line. Inset: Guinier plot of the experimental SAXS profile (fit included).

protein volume. For the hydrated 15-LOX-1 a volume $V_{\text{solution}} = 15.0 \times 10^4 \text{ \AA}^3$ was calculated as compared with $V_{\text{crystal}} = 9.2 \times 10^4 \text{ \AA}^3$ determined by X-ray crystallography. Nevertheless, the SAXS data indicate that under our experimental conditions the 15-LOX is monomeric, and that the scattering profiles can be used for more detailed structural analyses.

The theoretical SAXS profile and the $P(r)$ function calculated from the crystal structure using the program CRY SOL²⁸ are shown in Figures 2 and 3 (broken lines). The obvious discrepancy between the theoretical and experimental values for the radius of gyration ($R_G = 28.4 \text{ \AA}$ versus $R_G = 33.4 (\pm 0.5) \text{ \AA}$, respectively) and of the entire scattering

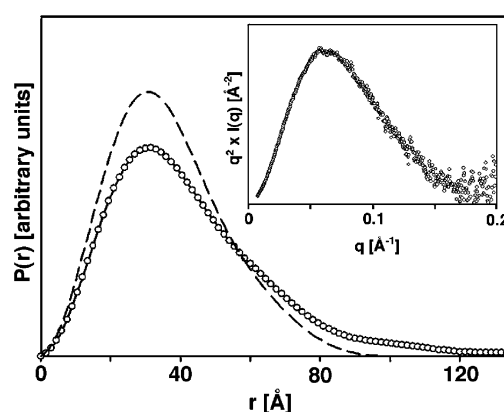


Figure 3. Distance distribution functions $P(r)$ calculated from the SAXS pattern. The experimental SAXS profile of the rabbit 15-LOX-1 and the theoretical profile calculated from the crystal structure as shown were used to calculate the $P(r)$ function (see Materials and Methods). Open circles indicate the experimental data, the broken line the theoretical profile evaluated by the program GNOM. Inset: Kratky plot of the experimental SAXS profile.

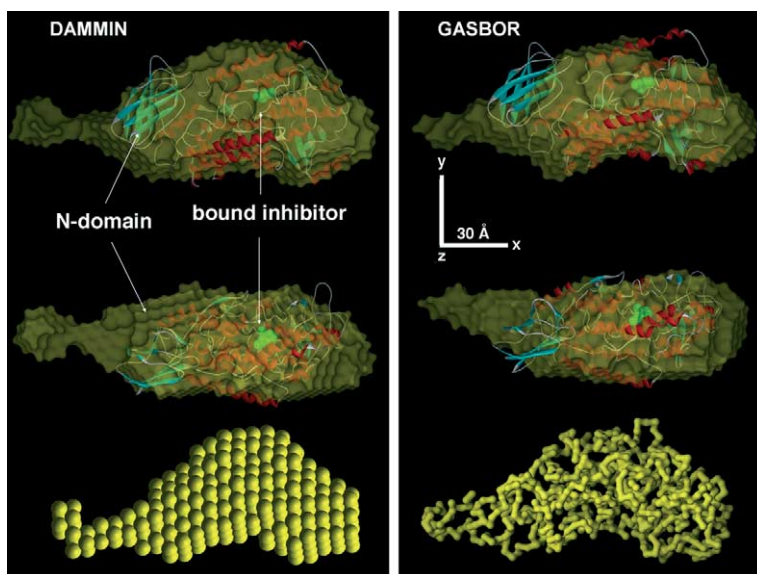


Figure 4. Superposition of the averaged low resolution models with the crystal structure. Low-resolution models for the 3D structure of the rabbit enzyme were calculated using two different methodological approaches (DAMMIN, left panel and GASBOR, right panel). The low-resolution models are displayed in a greenish transparent surface presentation. The secondary structural elements of the crystal structure (ribbon diagrams with turquoise β -sheets and red α -helices) are overlaid. The competitive inhibitor (3-(2-octylphenyl)propanoic acid) located in the substrate binding pocket is colored green. The middle panel shows the models of the upper panel rotated clockwise by 90° around the x -axis. The structures at the bottom represent the restored models.

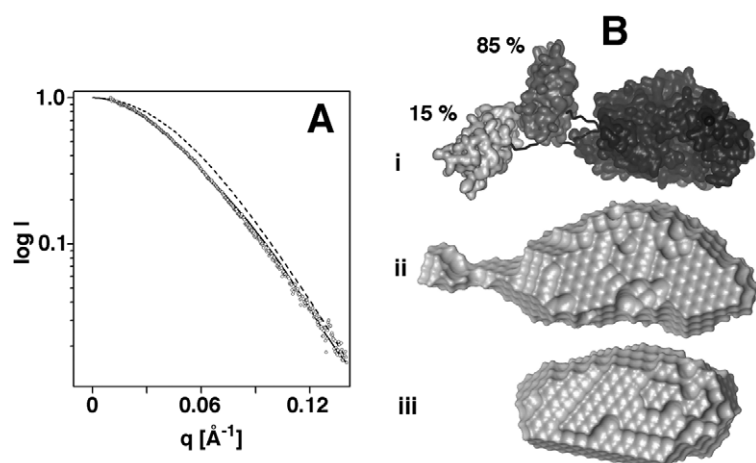
profile suggested detailed structural differences. The shape of the $P(r)$ function calculated for the experimental scattering curve suggests a more extended structure with a diameter of the molecule $D_{\max} = 135(\pm 7)$ Å. In comparison, a $D_{\max} = 100$ Å was calculated from the crystal structure (Figure 3). The tailing of the experimental $P(r)$ function provides evidence for a higher structural anisotropy of 15-LOX-1 in solution, although the maximum in the $P(r)$ function at 30 Å remains preserved. The most likely interpretation for the structural differences between the crystal and the solution structure is a high degree of interdomain movement. Extensive unfolding of the enzyme, which is likely to lead to a functional impairment of the enzyme appears unlikely because of two reasons. (i) The Kratky plot [$q^2 I(q)$ versus q] shown in Figure 3 (inset) exhibits the characteristics of a properly folded protein. In fact, Kratky plots of a globular particle constitute bell-shaped curves while an unfolded protein shows a plateau at larger q -values. (ii) According to our experience the 15-LOX-1 in aqueous solutions is fairly stable over a time period of one to two hours if the temperature is kept between 5 and 10 °C. In fact, under these conditions essential enzyme characteristics, such as catalytic efficiency (K_M , V_{\max}) or reaction specificity are not significantly altered. Hence, the obvious increase in the protein diameter indicated by the tailing of the $P(r)$ function is probably due to rearrangement of the two structural subunits relative to each other.

Solution structure of the rabbit 15-LOX-1

Reconstruction of the overall shape of the rabbit 15-LOX-1 from X-ray scattering data was achieved by two independent *ab initio* modeling methods (DAMMIN²⁹ and GASBOR³⁰). DAMMIN is particularly appropriate for objects displaying a sharp particle-solvent interface, which exactly

follow the Porod law. However, according to the $P(r)$ function extracted from the scattering data, the surface of 15-LOX-1 is not well defined and the X-ray coordinates support this conclusion. These structural properties prompted us to apply a second modeling approach (GASBOR). For both procedures the scattering profiles up to $q_{\max} = 0.21 \text{ \AA}^{-1}$ were used and five repetitive runs of modeling were carried out with each method. The single models show variations between independent runs with similar quality of fitting but multiple repetition of the modeling process significantly decreases the risk of inferring an erroneous low-resolution structure. Hence, the five single restored models were subjected to superposition and averaging by the program SUPCOMB.³¹ The averaged models exactly fit the experimental data with discrepancies $\chi = 1.6$ for DAMMIN and $\chi = 1.7$ for GASBOR.

From Figure 4 it can be seen that with both modeling procedures a similar low-resolution enzyme structure was obtained. However, comparing these solution structures with the X-ray coordinates of the LOX crystals three major aspects become evident. (i) The solvent structure of the catalytic domain did almost perfectly match the crystallographic data. (ii) The overall shape of the solvent structure is significantly stretched out (extended diameter), which is consistent with the shape of the $P(r)$ function. (iii) There is a central bending of the LOX molecule in the solution structure, which did not show up in the crystals. These overall shape characteristics are highly reproducible for all runs of structural modeling and with both *ab initio* modeling methods (see Figure 4, single models). The most probable explanation for the stretched-out shape of the solution structure may be a motional flexibility of the N-terminal β -barrel domain (related to the catalytic domain). In the crystal structure of the



stretched linker (AS111–AS121) is displayed as black tube. ii: Averaged low-resolution model calculated from the experimental SAXS curve. iii: Low-resolution model calculated from the theoretical SAXS curve of the crystal structure using the program DAMMIN. The models are displayed in surface presentation.

rabbit enzyme¹³ the β -barrel domain has a relatively high temperature factor. In soybean LOX-1 crystals the temperature factor of the β -barrel domain is also increased and some residues may even form external loops.¹¹ Following this line, the N-terminal domain of the 15-LOX-1 exhibits a high degree of motional freedom and the experimental SAXS curves result from the superposition of various protein conformations. To confirm this assumption, five different protein conformations have been constructed by stretching the interdomain linker (random coil consisting of amino acid residues 111–124). Different percentages of these notional protein constructs were combined and the corresponding scattering patterns were compared to the experimental SAXS curve. The best fit was observed using the automatic fit algorithm OLIGOMER†. Figure 5(A) shows the improvement in fitting ($\chi=1.9$) for the mixed SAXS profile (continuous line) in comparison to the crystal structure ($\chi=2.5$, broken line). The most appropriate result was received by superposition of a stretched conformation and a slightly open conformation with a volume fraction of 15% and 85%, respectively (Figure 5(B), panel i). This hypothetical protein construct reflects the experimental scattering profile and the structural features of our low-resolution model (Figure 5(B), panel ii). In contrast, the DAMMIN model calculated for the crystal structure (Figure 5(B), panel iii) was much more compact and lacks the central bending. In view of these results one may conclude that the experimental SAXS data are an average of various conformational states and the recovered low-resolution models represent an average in time and space.

Solution structure of the isolated catalytic domain

To strengthen our conclusion of the motional flexibility of the N-terminal domain we measured the solution SAXS profile of the isolated C-terminal domain of the rabbit 15-LOX-1 (catalytic domain comprising amino acid residues 115–662). For this purpose the N-terminal deletion mutant was created gene-technologically³² and the truncated protein was expressed as a His-tag fusion protein in *Escherichia coli*. After purification on Ni-agarose and Q-Sepharose open bed columns the recombinant enzyme mutant was characterized with respect to its functional characteristics (K_M , V_{max} , reaction specificity). Only minor differences in the kinetic parameters were observed when the truncated enzyme was compared with the complete recombinant 15-LOX-1.³² The final enzyme preparation was concentrated to 1 mg/ml and SAXS measurements were carried out at the synchrotron beamline under the same experimental conditions as outlined for the native enzyme. The experimental SAXS data were linear in the Guinier plot and revealed a radius of gyration $R_G=26.2(\pm 1.2)$ Å. The distance-distribution-function $P(r)$ has a bell-shaped appearance, which is typical for a spherical particle and a maximal diameter $D_{max}=80(\pm 5)$ Å was estimated (Figure 6, inset). Next, we compared the experimental data with the calculated SAXS profile of the atomic model of the catalytic domain created by deletion of the N-terminal domain (amino acid residues 1–114) in the crystal structure. The calculated scattering profile is almost identical with the experimental one and the high quality of fitting is indicated by the low discrepancy parameter $\chi=1.4$ (Figure 6, continuous line). A theoretical radius of gyration $R_G=24.6$ Å was determined, which is close to the experimental value. The theoretical $P(r)$ function with the $D_{max}=84$ Å (Figure 6 inset, continuous line) matches the experimental data perfectly. These results suggest that the overall

† Svergun, D. I., Sokolova, A. V. & Volkov, V. V. (2003). OLIGOMER—<http://www.embl-hamburg.de/ExternalInfo/Research/Sax/>

Figure 5. Averaged low-resolution models of the rabbit 15-LOX-1. (A) The low-angle experimental SAXS profile of the rabbit 15-LOX-1 (open circles) in comparison to the theoretical profile calculated for the crystal structure (broken line) and for the hypothetical mixture of two protein conformations (continuous line) as illustrated in Figure 7. (B) i: The two conformations of 15-LOX-1, which were used for the calculation of a mixed SAXS profile yielding the best fit to the experimental SAXS profile at a percentage ratio of 15% to 85%, are shown as surface presentation. The

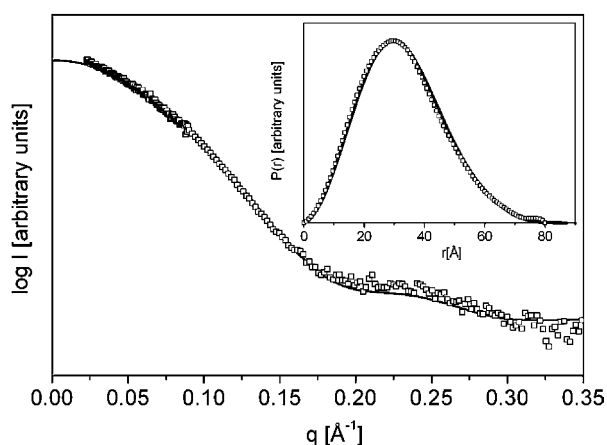


Figure 6. Comparison of the experimental and theoretical SAXS profiles of the C-terminal domain from the rabbit 15-LOX-1. Experimental data are indicated by open squares and the theoretical SAXS profile calculated from the atomic structure is given by the continuous line. Inset: Distance distribution functions $P(r)$ calculated from the SAXS profiles. Open squares indicate $P(r)$ calculated for the experimental data, the continuous line indicates the theoretical $P(r)$ evaluated by the program GNOM.

structure of the isolated catalytic domain in solution appears to be identical to that in the crystal structure and that the changes observed in the solution structure of the entire 15-LOX-1 molecule

may be due to a high degree of motion flexibility of the N-terminal domain.

Structural flexibility and membrane binding

To test our hypothesis on the structural flexibility of the N-terminal β -barrel domain and interdomain movement we carried out membrane binding assays using wild-type and a mutant 15-LOX-1 species. LOXs exhibit a tendency for membrane association and surface exposed hydrophobic amino acid residues (Tyr15, Phe70, Leu71, Trp181, Leu195 for the rabbit 15-LOX^{32,33} and Trp14, Trp76, Trp103 for the human 5-LOX³⁴) have been implicated. Sequence alignments of these two enzymes indicate that Trp14 and Trp76 of the human 5-LOX align in the region of Tyr15 and Phe70 of the rabbit enzyme. Trp103 of the 5-LOX (membrane binding determinant) aligns with Trp100 of the rabbit enzyme.³³ When we looked for the position of Trp100 in the crystal structure of the rabbit enzyme we identified this amino acid as constituent of the interdomain contact plane. Thus, large parts of this hydrophobic residue are shielded by the catalytic subunit (Figure 7(A)). In fact, in the crystal structure less than 10% of this hydrophobic side-chain is solvent exposed as opposed to the other sequence determinants of membrane binding (Tyr15, 50%; Phe70, 35%; Leu71, 55%). Because of this shielding Trp100 was unlikely to contribute to membrane binding. However, if the β -barrel domain is

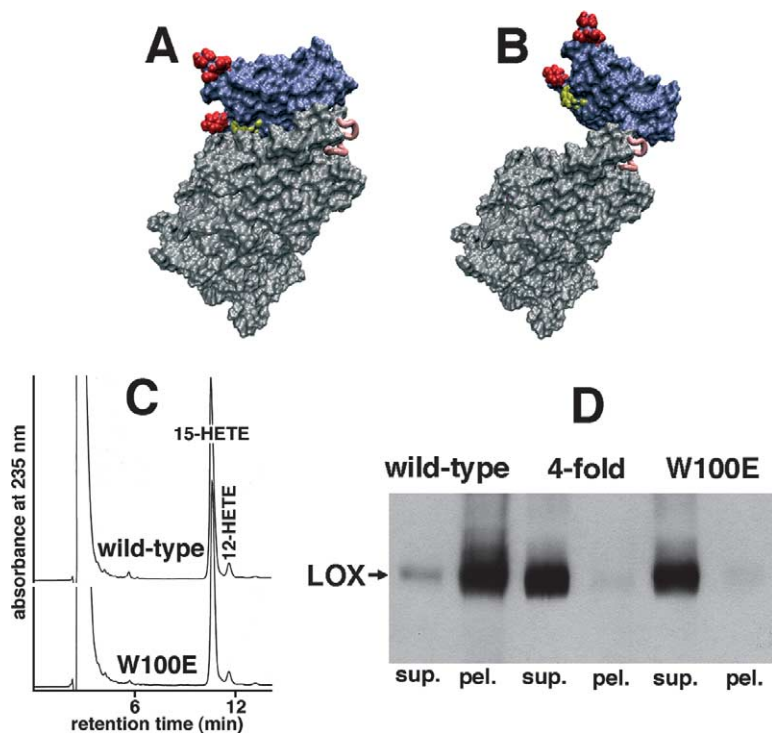


Figure 7. Membrane binding of wild-type and mutant rabbit 15-LOX-1 species. (A) Surface structure of the crystallized rabbit 15-LOX-1 indicating interdomain interaction. The N-terminal β -barrel domain is shown in blue, the catalytic domain in grey and the interdomain linking peptide in magenta. The sequence determinants for membrane binding that are located in the N-terminal domain (Tyr15, Phe70 and Leu71) are colored in red. Trp100 (potential additional determinant for membrane binding) is given in yellow. This view indicates the limited solvent exposure of Trp100 in the crystal structure. (B) Relaxed surface structure, in which the β -barrel domain is dislocated from the catalytic subunit. Here Trp100 is more than 30% solvent exposed. (C) HPLC analysis of the reduced arachidonic acid oxygenation product formed by the recombinant wild-type 15-LOX-1 and its Trp100Glu mutant. This product

pattern is similar to that of the native enzyme. Hence, arachidonic acid oxygenation is completely enzyme-controlled. (D) Membrane binding of wild-type and mutant 15-LOX-1 isoforms. The membrane binding assays were carried out as described in Materials and Methods. Membrane (pel.) and supernatant (sup.) fractions were probed by immunoblotting for their 15-LOX content. Fourfold: Y15E + F70H + L71K + L195E quadruple mutant, which does not exhibit major membrane binding activity.³³

dislocated from the catalytic subunit (Figure 7(B)) Trp100 becomes more surface exposed (more than 30% solvent exposure) and in this case, it may act as a membrane binding determinant. To find out whether or not Trp100 is important for membrane binding we mutated this amino acid to a negatively charged Glu (W100E), expressed the wild-type and mutant enzyme species as a His-tag fusion protein in *E. coli*, purified the recombinant enzyme species and tested them in an *in vitro* membrane binding assay. A similar strategy has previously been used to test the importance of other amino acid residues (Tyr15, Phe70, Leu71, Trp181, Leu195).³³ To exclude the possibility that the Trp100Glu exchange severely alters the overall protein structure the mutant enzyme was characterized with respect to basic enzymatic properties. The mutant exhibited a similar catalytic activity for arachidonic acid oxygenation as the wild-type enzyme (data not shown) and converted this substrate predominantly to 15S-HpETE (Figure 7(C)). These data suggest that no major structural alterations have been introduced by this mutation.

For our membrane-binding assay the LOX species were incubated with sub-mitochondrial particles (SMPs) for a certain time period, the membranes were spun down and the LOX content was determined by immunoblotting in the membrane and in the supernatant fraction. As indicated in Figure 7(D) the wild-type enzyme was predominantly found in the membrane fraction, indicating a high degree of membrane binding. In contrast, the Trp100Glu mutant was almost exclusively recovered from the supernatant fraction, suggesting a severe loss in membrane binding capability. A similar behavior was found for the Y15E + F70H + L71K + L195E quadruple mutant and these data are consistent with previous findings.³³ The loss of the membrane binding activity of the Trp100Glu mutant can hardly be explained in the light of the crystal structure. However, the data become plausible if one allows a substantial movement of the N-terminal domain relative to the catalytic subunit, which reduces the degree of shielding of Trp100 and leads to solvent exposure of the interdomain contact planes of both the N-terminal and C-terminal domains.

Discussion

The crystal structures of two different soybean LOX-isoforms (isozyme 1 and 3) are currently available.^{10–12} In addition, the 3D structure of a rabbit 15-LOX-1-inhibitor complex has been solved at 2.4 Å resolution.¹³ Unfortunately, up to now no solution structure has been published for any LOX isoform. For this paper we investigated the low-resolution structure of the rabbit 15-LOX-1 in aqueous solution by SAXS measurements and found three major differences to the crystal structure. (i) In aqueous solution the radius of gyration of the enzyme is larger than that in the crystal

structure ($R_G = 33.4(\pm 0.5)$ Å versus $R_G = 28.4$ Å, respectively). (ii) The overall shape of the solution structure is significantly stretched out. In fact, it resembles an elliptic cylinder with a height of 135 Å. In contrast, this value is only 100 Å for the crystal structure. (iii) There is a bending in the center of the solution structure, which does not show up in the crystal structure.

The mechanistic reasons for these structural differences are likely to be related to the degree of enzyme hydration. Protein hydration may induce stretching of surface-exposed loop regions and thus, may lead to a higher degree of interdomain movement.³⁵ In the case of 15-LOX-1 we could show that the solution structure of the separated C-terminal catalytic domain was very similar to that obtained by X-ray crystallography. Hence, the structural flexibility of the complete protein is most probably due to a dislocation of the N-terminal domain (Scheme 1).

In fact, our membrane binding studies suggest that interdomain movement may lead to surface exposure of Trp100. Since, in the crystal structure, the catalytic domain shields Trp100 it may only act as membrane binding determinant if interdomain movement increases its solvent exposure. Hence, the results of our membrane binding studies may be considered as indirect evidence for the motional flexibility of the 15-LOX solution structure.

The crystal structure of the rabbit 15-LOX was solved in the presence of a competitive inhibitor, which is located at the active site and thus, the enzyme-inhibitor complex represents an inactive form of the protein. It is conceivable to assume that binding of substrates and/or inhibitors may impair the structural flexibility of the protein and thus, may prevent relaxation of the 3D structure. Unfortunately, SAXS measurements of the enzyme-inhibitor complex could not be carried out, since this inhibitor is not commercially available and other inhibitors have not been tested with respect to their impact on the crystal structure. It is important to note that 15-LOX was crystallized from highly concentrated protein solutions at high ionic strength (about 0.5 M Li_2SO_4). Such high LOX and salt concentrations, which are far above the physiological range, might force the protein into a more rigid conformation. In contrast, our SAXS experiments were carried out at much lower LOX and salt concentrations and this may contribute to the structural differences. The characteristic stretching of the complete enzyme structure and the flexibility of the N-terminal β -barrel domain might also be a reason for the aggregation of the protein at higher concentrations and higher temperatures, as observed during our preliminary SAXS experiments. Intermolecular interactions between the exposed hydrophobic regions are conceivable to occur with the objective to hide the hydrophobic amino acid residues from water contact.

As indicated above the structural peculiarities of the relaxed enzyme structure might be interpreted as a consequence of motion of the N-terminal

β -barrel domain relative to the catalytic subunit. In principle, two different kinds of movement appear possible (Scheme 1). (i) Linear movement of the entire β -barrel domain away from the catalytic subunit, which causes maximal stretching of the enzyme molecule (B). (ii) Swing-out of the β -barrel domain articulated by the random coil (C). This kind of movement leads to stretching of the enzyme molecule but may also induce bending of the overall shape. The major precondition for the two kinds of movement is the unusually long random coil structure that connects the N-terminal and the C-terminal domains. The crystal structure (condensed form) and the maximally stretched enzyme (relaxed form) are limit structures, but in aqueous solution intermediate conformations are likely to occur. Thus, the solution structure of the 15-LOX-1 constructed from the SAXS data may represent an average of various conformational states, in which the distance between the two domains (stretching of the molecule) and their relative orientation (bending of the molecule) are different. Whether the different structural states (relaxed or condensed form of the enzyme) exhibit different catalytic properties remains to be investigated in the future.

The flexibility of the solution structure of the rabbit 15-LOX-1, in particular the higher degree of motional freedom of the N-terminal β -barrel domain, may be of biological relevance for membrane binding but also for regulation of the catalytic activity. It has been reported that the N-terminal β -barrel domain of LOX is not required for the catalytic activity. In fact, when limited proteolysis was carried out on the soybean LOX-1 the β -barrel domain was cleaved off. After chromatographic separation the isolated catalytic domain exhibited an augmented catalytic activity when compared with native enzyme.³⁶ This result was interpreted as a regulatory function of the N-terminal β -barrel domain. In the light of our findings it may be speculated that the movement of the β -barrel domain may repress the catalytic efficiency of the LOX.³⁶ Truncation of the rabbit 15-LOX N-terminal domain did also lead to catalytically active enzyme species.³² However, in this case the catalytic activity was impaired. The reasons for this antiparallel behavior of the two LOX isoforms have not been investigated in detail but it might be possible that the interdomain interactions may involve positive and/or negative regulatory elements in different isoforms.

Materials and Methods

Chemicals

The chemicals used were from the following sources: (5Z,8Z,11Z,14Z)-eicosa-5,8,11,14-tetraenoic acid (arachidonic acid), EDTA, imidazole and sodium borohydride from Serva (Heidelberg, Germany); ampicillin from Gibco (Eggenstein, Germany); Kanamycin, glycerol, DTT (dithiothreitol), TCA (trichloroacetic acid), calcium chloride (99.99%) and sucrose from Sigma-Aldrich

(Deisenhofen, Germany); HPLC reference compounds (12S,5Z,8Z,10E,14Z)-12-hydroxy-5,8,10,14-eicosatetraenoic acid (12S-HETE), (15S,5Z,8Z,11Z,13E)-15-hydroxy-5,8,11,13-eicosatetraenoic acid (15S-HETE)] from Cayman Chem. (distributed by Alexis GmbH, Grünberg, Germany); ammonium sulfate from Merck (Darmstadt, Germany); HPLC solvents from Baker (Deventer, The Netherlands). Restriction enzymes were purchased from New England Biolabs (Schwalbach, Germany). Phage T4 ligase, PWO-polymerase and sequencing kits were obtained from Boehringer Mannheim (Mannheim, Germany) and the *E. coli* strain M15[prep4] was purchased from Qiagen (Hilden, Germany). Oligonucleotide synthesis was carried out by TiB-Molbiol (Berlin, Germany).

Preparation of the native rabbit 15-LOX and partial characterization of the enzyme

The rabbit 15-LOX was prepared from a stroma-free supernatant of a reticulocyte-rich blood cell suspension by sequential fractionated ammonium sulfate precipitation, hydrophobic interaction chromatography (Biogel SEC Phenyl-5-PW column; Biorad, Munich, Germany) and anion exchange chromatography (Resource-Q column; Pharmacia, Uppsala, Sweden).²⁴

Bacterial expression and purification of wild-type and mutant recombinant 15-LOX species

The recombinant wild-type 15-LOX and mutants were expressed in *E. coli* as His-tagged fusion proteins and purified over Ni-agarose and Q-Sepharose.³² For storage the enzyme preparations were supplemented with 10% glycerol and stored at -80°C .

Site-directed mutagenesis

Site-directed point mutations were performed using the QuickChange™ Site-Directed Mutagenesis Kit (Stratagene, Amsterdam, The Netherlands) and the primary structures of mutated plasmids were confirmed by DNA sequencing. For the mutants five to ten clones were screened by restriction mapping and activity assays to identify catalytically active LOX-positive clones. N-terminal truncation of the rabbit 15-LOX-1 was carried out as described.³² The enzyme was expressed as a His-tag fusion protein in *E. coli* and purified to apparent homogeneity by sequential chromatography on Ni-agarose and Q-Sepharose open bed columns. The basic enzymatic parameters (K_M , V_{max} , reaction specificity) of the truncation mutant were comparable to those of the recombinant wild-type enzyme.

Arachidonic acid oxygenase activity

Arachidonic acid oxygenase activity of wild-type and mutant 15-LOX species was assayed by HPLC quantification of the oxygenation products. The assay mixture consisted of a 10 mM Tris-HCl buffer (pH 7.4) and 0.1 mM arachidonic acid as substrate (0.5 ml total assay volume). The reaction was stopped by the addition of 0.5 ml ice-cold methanol, the hydroperoxides formed were reduced to the more stable hydroxy compounds with sodium borohydride and the sample was acidified to pH 3 (with acetic acid). After removing the precipitate by centrifugation aliquots of the clear supernatant were injected to RP-HPLC for isolation and quantification of the reaction products.

HPLC analysis of the LOX products

HPLC was performed on a Shimadzu system connected to an Agilent 1100 diode array detector (Agilent Technologies, Waldbronn, Germany). Reverse phase-HPLC was carried out on a Nucleosil C-18 column (Macherey-Nagel, KS-system, 250 mm × 4 mm; 5 μm particle size) coupled with an appropriate guard-column (30 mm × 4 mm; 5 μm particle size). For analysis of the hydroxylated fatty acids a solvent system of methanol/water/acetic acid (80 : 20 : 0.1, by vol.) was used at a flow rate of 1 ml/minute. The chromatographic scale was calibrated for conjugated dienes by injecting known amounts of 15-HETE (five-point calibrations). The chromatograms were recorded at 235 nm (quantification of conjugated dienes). For enantiomer separation of 15-HETE chiral phase-HPLC was performed on a Chiralcel OD column (250 mm × 4 mm; 5 μm particle size; Diacel Chemical Ind. Ltd) with the solvent system *n*-hexane/2-propanol/acetic acid (100 : 5 : 0.1, by vol.) and a flow rate of 1 ml/minute.

Membrane binding assay

Membrane binding was carried out as described.³² Briefly, 200 μg of sub-mitochondrial particles were incubated at room temperature with 1 μg of recombinant 15-LOX (wild-type or mutant enzyme species) in 50 mM Hepes buffer (pH 7.4) containing 150 mM NaCl and 1 mM DTT (total assay volume 25 μl). After a five minute incubation period the samples were underlaid with a 0.1 ml sucrose cushion (500 mM sucrose in the same buffer) and centrifuged for 15 minutes at 100,000g in a Beckmann tabletop centrifuge (4 °C). The pellet of this centrifugation step represented LOX-loaded SMPs. The supernatant was carefully removed, transferred to a separate tube and ovalbumin was added to reach a final concentration of 60 μg/ml. The supernatant proteins were then precipitated with trichloroacetic acid (TCA) reaching a final concentration of 10% and spun down by centrifugation for 20 minutes at 20,000g. The supernatant of the centrifugation step was discarded and the two pellets (100,000g pellet and 20,000g pellet) were reconstituted in 25 μl of twofold concentrated electrophoresis loading buffer (0.58 M sucrose, 280 mM Tris-base, 211 mM Tris-HCl, 139 mM SDS, 1 mM EDTA, 0.44 mM Serva blue G250, and 200 mM DTT). After heating to 95 °C for five minutes aliquots (4 μl) were loaded onto SDS-PAGE. After electrophoresis the proteins were blotted to a nitrocellulose membrane by a semi-dry blotting technique and the blots were probed with a mouse anti-RGS-His-tag antibody (Qiagen, Hilden, Germany). As secondary antibody a peroxidase-conjugated anti-mouse IgG antibody (Sigma, Deisenhofen, Germany) was used. The blots were visualized by treating them with the Western Lightning Chemiluminescence Plus reagent (Perkin Elmer, Boston, USA). The intensity of the immunoreactive bands was quantified densitometrically using the Phoretix 1D software package (Phoretix International, Newcastle, UK).

Small-angle X-ray scattering (SAXS)

As protein aggregation constitutes a major problem in structure reconstitution from SAXS profiles preliminary measurements were carried out on a Hecus SAXS camera (HECUS X-ray Systems, Graz, Austria) in order to investigate the aggregation tendency of 15-LOX

depending on protein concentration and temperature. The camera was equipped with a thermostatically controlled sample holder. The measurements were performed at 10 °C and 20 °C, respectively, using a quartz capillary with a volume of 40 μl and an inner diameter of 1.0 mm. A Ni-filtered primary X-ray beam was generated by a water-cooled rotating Cu anode generator (Rigaku Corp., Japan). For initial experiments the SAXS patterns of the native rabbit LOX were measured at two different protein concentrations (0.7 mg/ml and 5 mg/ml) in a scattering vector range (*q*-range) of 0.01 Å⁻¹–0.12 Å⁻¹. The exposure time of the protein solutions to the X-ray beam was usually two hours for a single measurement. The scattering pattern of the solution buffer (50 mM Tris-HCl, 30 mM NaCl (pH 7.2)) was determined independently and then subtracted from that of the sample.

For more detailed studies SAXS measurements were carried out on the ID02 beamline at the European Synchrotron Radiation Facility (ESRF, Grenoble, France). Here a wavelength of 1.0 Å was adjusted and the sample-detector distance was 3.0 m, which leads to scattering vectors *q* ranging from 0.015 to 0.21 Å. The detector was an X-ray intensified optically coupled CCD camera, and 70 successive frames of 0.5 second exposure time (5 second intermission between each frame) were recorded for each sample. To avoid radiation-induced protein damage the enzyme solution was continuously circulated through a quartz capillary. Each frame was carefully checked for possible bubble formation or radiation-induced aggregation. If such effects were not observed, the individual frames were averaged. The measuring system was calibrated with a Lupolen sample. Immediately before measurements the protein samples were filtered through a Millex Microfilter membrane (pore size 0.22 μm) to eliminate existing aggregates. Here again background scattering (50 mM Tris-HCl, 30 mM NaCl (pH 7.2)) was quantified before or after measurements of the protein sample and the signals obtained were subtracted from the protein SAXS patterns. All experiments were performed at 10 °C.

Data processing

The resulting scattering data were subjected to indirect Fourier transformation using the program GNOM.³⁷ The raw data recorded by the Kratky compact camera with slit collimation were additionally de-smearred according to slit width and slit length profiles of the primary beam. Radii of gyration (*R_G*) were determined by Guinier approximation from the low *q*-regions of the scattering profiles, yielding also the scattering intensity extrapolated to the zero angle *I*₀.³⁸ *I*₀ on the absolute intensity scale was used to calculate the molecular mass (*M_w*) of 15-LOX using equation (1):

$$I_0 = \frac{cM_w}{N_a} [(\rho_{\text{prot}} - \rho_{\text{sol}})\bar{v}_{\text{prot}}]^2 \quad (1)$$

where *c* is the protein concentration, *M_w* the molecular mass of the protein and *N_a* Avogadro's number. The ρ_{prot} and ρ_{sol} terms represent the electron density distributions of protein and solvent, respectively, calculated as: $\frac{0.282 \times 10^{-12} \times n_{\text{electron}}}{v_{\text{mol}}} \times N_a$, where the constant 0.282×10^{-12} is the radius of the electron, *n_{electron}* the number of electrons in one enzyme molecule with the volume *v_{mol}*. The \bar{v}_{prot} value is the partial specific volume calculated as *v_{mol}*/*M_w*. The calculated *M_w* was compared to the theoretical *M_w* obtained from the known protein sequence. The GNOM program was also used to compute the pair-distance

distribution function $P(r)$, which represents the probability of finding a point within the particle at a distance r from a given point. Integrating this probability over the surface of a sphere with radius r and over the volume V yields the function $P(r)$ as expressed by:

$$P(r) = \frac{1}{2\pi^2} \int_0^\infty r q I(q) \sin(rq) dq \quad (2)$$

This approach offers an alternative calculation of R_G and I_0 , which is based on the entire scattering curve³⁸ and gives the maximum dimension of the macromolecule D_{\max} as distance when the $P(r)$ function approaches zero.

Ab initio deconvolution of the SAXS profiles

The low-resolution shape of 15-LOX was restored from the experimental data by two independent software programs DAMMIN²⁹ and GASBOR.³⁰ The scattering profiles up to $q_{\max} = 0.21 \text{ \AA}^{-1}$ were used for the fit. The DAMMIN method calculates the scattering intensities from a multiphase model of a particle built up from a finite number of dummy beads that are characterized by the configuration vector assigning the beads to a specific phase or to the solvent. The method starts searching for a model in a volume filled by uniformly hexagonally packed beads, with dimensions selected according to the resolution of the scattering profile and taking into account the dimension of the initial search object. GASBOR searches a chain-compatible spatial distribution of an exact number of dummy residues, which corresponds to the distribution of C^α atoms of amino acid residues. The calculation of the scattering intensity from the model is based on the Debye formula.³⁹ In this fitting approach the number of amino acid residues of the protein must be specified. The programs search for the optimal model configuration, minimizing the discrepancy function:

$$f(X) = \chi^2 + \alpha P(X) \quad (3)$$

between calculated and experimental curves using the simulated annealing method.⁴⁰ In this equation, X represents the discrepancy between calculated and experimental curves, and $\alpha P(X)$ constitutes a looseness penalty with positive weight for $\alpha > 0$. The aim of this method is to modify the coordinates of the beads randomly, while always approaching the configurations that decrease the energy $f(X)$.

Calculation of a theoretical SAXS profile from the crystal structure

The crystallographic coordinates of the rabbit 15-LOX-1¹³ were used as the atomic model and the theoretical scattering curve was calculated using the program CRY SOL.²⁸ This method surrounds the macromolecule with a 3.0 Å hydration layer, which exhibits a slightly higher electron density than the solvent.⁴¹ The final scattering intensity is calculated as the addition of scattering of the particle in vacuum and the hydration layer followed by subtraction of scattering from the excluded volume. Finally, the theoretical scattering profile was compared to the experimental SAXS data. To test the reliability of our modeling approaches and to support our mechanistic conclusion the theoretical scattering profile obtained for the crystal structure was subjected to the *ab initio* modeling approaches. The quality of fit for all atomic models, as well as for the low-resolution models

with the experimental data was determined using the discrepancy χ defined according to Konarev *et al.*⁴²

Miscellaneous methods

Protein concentration was determined with the Roti-Quant detection system (Roth, Karlsruhe, Germany) that is based on the Bradford method. SDS-PAGE was carried out according to a standard protocol in a 10% (w/v) polyacrylamide gel. Gel filtration was performed on a Pharmacia FPLC system equipped with a Superose 12 column. SMPs, which mainly constitute inside-out vesicles of the inner mitochondrial membrane, were prepared as described.⁴³ Structural modeling of the rabbit 15-LOX-arachidonic acid complex was carried out with the Hyperchem 5.0 software package. Amino acids, the coordinates of which have not been determined in the crystal structure, were modeled in using the Swiss-Pdb software† followed by energy minimization of the side-chains.

Acknowledgements

The authors thank Mrs C. Gerth for excellent technical assistance, Mr J. Saam for fruitful discussions of the structural aspects and Véronique Receveur-Bréchet for critical reading of the manuscript and for her support during SAXS measurements. Furthermore, we are indebted to Stéphanie Finet and the synchrotron staff at ESRF, Grenoble, France, for the use of ID02 beamline and for technical assistance in the SAXS measurements. Financial support for this study was provided by Deutsche Forschungsgemeinschaft (Ku961/7-1/2) and by a grant from the Fonds zur Förderung der wissenschaftlichen Forschung (P16479-N11) (to R.P.).

References

1. Brash, A. R. (1999). Lipoxygenases: occurrence, functions, catalysis, and acquisition of substrate. *J. Biol. Chem.* **274**, 23679–23682.
2. Samuelsson, B., Dahlen, S. E., Lindgren, J. A., Rouzer, C. A. & Serhan, C. N. (1987). Leukotrienes and lipoxins: structures, biosynthesis, and biological effects. *Science*, **237**, 1171–1176.
3. Funk, C. D. (2001). Prostaglandins and leukotrienes: advances in eicosanoid biology. *Science*, **294**, 1871–1875.
4. Serhan, C. N., Takano, T., Gronert, C., Chiang, N. & Clish, C. B. (1999). Lipoxin and aspirin-triggered 15-epi-lipoxin cellular interactions anti-inflammatory lipid mediators. *Clin. Chem. Lab. Med.* **37**, 299–309.
5. Rapoport, S. M., Schewe, T. & Thiele, B. J. (1990). Maturation breakdown of mitochondria and other organelles in reticulocytes. *Blood Cell. Biochem.* **1**, 151–194.
6. van Leyen, K., Duvoisin, R. M., Engelhardt, H. &

† <http://www.expasy.ch/spdbv>

- Wiedmann, M. (1998). A function for lipoxygenase in programmed organelle degradation. *Nature*, **395**, 392–395.
7. Pidgeon, G. P., Kandouz, M., Meram, A. & Honn, K. V. (2002). Mechanisms controlling cell cycle arrest and induction of apoptosis after 12-lipoxygenase inhibition in prostate cancer cells. *Cancer Res.* **62**, 2721–2727.
 8. Cathcart, M. K. & Folcik, V. A. (2000). Lipoxygenases and atherogenesis: protection versus pathogenesis. *Free Rad. Biol. Med.* **28**, 1726–1734.
 9. Klein, R. F., Allard, J., Avnur, Z., Nikolcheva, T., Rotstein, D., Carlos, A. S. *et al.* (2004). Regulation of bone mass in mice by the lipoxygenase gene Alox15. *Science*, **303**, 229–232.
 10. Boyington, J. C., Gaffney, B. J. & Amzel, L. M. (1993). The three-dimensional structure of an arachidonic acid 15-lipoxygenase. *Science*, **260**, 1482–1486.
 11. Minor, W., Steczko, J., Stec, B., Otwinowski, Z., Bolin, J. T., Walter, R. & Axelrod, B. (1996). Crystal structure of soybean lipoxygenase L-1 at 1.4 Å resolution. *Biochemistry*, **35**, 10687–10701.
 12. Skrzypczak-Jankun, E., Amzel, L. M., Kroa, B. A. & Funk, M. O., Jr (1997). Structure of soybean lipoxygenase L3 and a comparison with its L1 isoenzyme. *Proteins: Struct. Funct. Genet.* **29**, 15–31.
 13. Gillmor, S. A., Villasenor, A., Fletterick, R., Sigal, E. & Browner, M. F. (1997). The structure of mammalian 15-lipoxygenase reveals similarity to the lipases and the determinants of substrate specificity. *Nature Struct. Biol.* **4**, 1003–1009.
 14. Pham, C., Jankun, J., Skrzypczak-Jankun, E., Flowers, R. A., II & Funk, M. O. (1998). Structural and thermochemical characterization of lipoxygenase-catechol complexes. *Biochemistry*, **37**, 17952–17957.
 15. Skrzypczak-Jankun, E., Bross, R. A., Carroll, R. T., Dunham, W. R. & Funk, M. O. (2001). Three dimensional structure of a purple lipoxygenase. *J. Am. Chem. Soc.* **123**, 10814–10820.
 16. Borbulevych, O. Y., Jankun, J., Selman, S. H. & Skrzypczak-Jankun, E. (2004). Lipoxygenase interactions with natural flavonoid, quercetin, reveal a complex with protocatechuic acid in its X-ray structure at 2.2 Å resolution. *Proteins: Struct. Funct. Genet.* **54**, 13–19.
 17. Hemak, J., Gale, D. & Brock, T. G. (2002). Structural characterization of the catalytic domain of the human 5-lipoxygenase enzyme. *J. Mol. Model.* **8**, 102–112.
 18. Borngräber, S., Browner, M., Gillmor, S., Gerth, C., Anton, M., Fletterick, R. & Kühn, H. (1999). Shape and specificity in mammalian 15-lipoxygenase active site. The functional interplay of sequence determinants for the reaction specificity. *J. Biol. Chem.* **274**, 37345–37350.
 19. Feigin, L. A. & Svergun, D. I. (1987). *Structural Analysis by Small-angle X-ray and Neutron Scattering*. Plenum Press, New York.
 20. Svergun, D. I. & Koch, M. H. (2002). Advances in structure analysis using small-angle scattering in solution. *Curr. Opin. Struct. Biol.* **12**, 654–660.
 21. Vachette, P., Koch, M. H. & Svergun, D. I. (2003). Looking behind the beamstop: X-ray solution scattering studies of structure and conformational changes of biological macromolecules. *Methods Enzymol.* **374**, 584–615.
 22. Koch, M. H., Vachette, P. & Svergun, D. I. (2003). Small-angle scattering: a view on the properties, structures and structural changes of biological macromolecules in solution. *Quart. Rev. Biophys.* **36**, 147–227.
 23. Hammel, M., Kriechbaum, M., Gries, A., Kostner, G. M., Laggner, P. & Prassl, R. (2002). Solution structure of human and bovine β 2-glycoprotein I revealed by small-angle X-ray scattering. *J. Mol. Biol.* **321**, 85–97.
 24. Kühn, H., Barnett, J., Grunberger, D., Baecker, P., Chow, J., Nguyen, B. *et al.* (1993). Overexpression, purification and characterization of human recombinant 15-lipoxygenase. *Biochim. Biophys. Acta*, **1169**, 80–89.
 25. Rapoport, S. M., Schewe, T., Wiesner, R., Halangk, W., Ludwig, P., Janicke-Höhne, M. *et al.* (1979). The lipoxygenase of reticulocytes. Purification, characterization and biological dynamics of the lipoxygenase; its identity with the respiratory inhibitors of the reticulocyte. *Eur. J. Biochem.* **96**, 545–561.
 26. Perez, J., Vachette, P., Russo, D., Desmadril, M. & Durand, D. (2001). Heat-induced unfolding of neocarzinostatin, a small all-beta protein investigated by small-angle X-ray scattering. *J. Mol. Biol.* **308**, 721–743.
 27. Akiyama, S., Takahashi, S., Kimura, T., Ishimori, K., Morishima, I., Nishikawa, Y. & Fujisawa, T. (2002). Conformational landscape of cytochrome c folding studied by microsecond-resolved small-angle x-ray scattering. *Proc. Natl Acad. Sci. USA*, **99**, 1329–1334.
 28. Svergun, D., Barberato, C. & Koch, M. H. J. (1995). CRYSOLE—a program to evaluate X-ray solution scattering of biological macromolecules from atomic coordinates. *J. Appl. Crystallog.* **28**, 768–773.
 29. Svergun, D. I. (1999). Restoring low resolution structure of biological macromolecules from solution scattering using simulated annealing. *Biophys. J.* **76**, 2879–2886.
 30. Svergun, D. I., Petoukhov, M. V. & Koch, M. H. (2001). Determination of domain structure of proteins from X-ray solution scattering. *Biophys. J.* **80**, 2946–2953.
 31. Kozin, M. B. & Svergun, D. I. (2001). Automated matching of high- and low-resolution structural models. *J. Appl. Crystallog.* **34**, 33–41.
 32. Walther, M., Anton, M., Wiedmann, M., Fletterick, R. & Kuhn, H. (2002). The N-terminal domain of the reticulocyte-type 15-lipoxygenase is not essential for enzymatic activity but contains determinants for membrane binding. *J. Biol. Chem.* **277**, 27360–27366.
 33. Walther, M., Wiesner, R. & Kuhn, H. (2004). Investigations into calcium-dependent membrane association of 15-lipoxygenase-1. Mechanistic roles of surface exposed hydrophobic amino acids and calcium. *J. Biol. Chem.* **279**, 3717–3725.
 34. Kulkarny, S., Das, S., Funk, C. D., Murray, D. & Cho, W. (2002). Molecular basis of the specific subcellular localization of the C2-like domain of 5-lipoxygenase. *J. Biol. Chem.* **277**, 13167–13174.
 35. Affleck, R., Xu, Z. F., Suzawa, V., Focht, K., Clark, D. S. & Dordick, J. S. (1992). Enzymatic catalysis and dynamics in low-water environments. *Proc. Natl Acad. Sci. USA*, **89**, 1100–1104.
 36. Maccarrone, M., Salucci, M. L., van Zadelhoff, G., Malatesta, F., Veldink, G., Vliegenthart, J. F. G. & Finazzi-Agro, A. (2001). Tryptic digestion of soybean lipoxygenase-1 generates a 60 kDa fragment with improved activity and membrane binding ability. *Biochemistry*, **40**, 6819–6827.
 37. Svergun, D. I. (1992). Determination of the regularization parameter in indirect-transform methods using perceptual criteria. *J. Appl. Crystallog.* **25**, 495–503.

38. Glatter, O. (1982). Data treatment. In *Small Angle X-ray Scattering* (Glatter, O. & Kratky, O., eds), Academic Press, London, New York, Paris.
39. Debye, P. (1915). Zerstreung von Röntgenstrahlen. *Ann. Phys.* **46**, 809–823.
40. Kirkpatrick, S., Gelatt, C. D., Jr & Vecchi, M. P. (1983). Optimization by simulated annealing. *Science*, **220**, 671–680.
41. Svergun, D. I., Richard, S., Koch, M. H., Sayers, Z., Kuprin, S. & Zaccai, G. (1998). Protein hydration in solution: experimental observation by X-ray and neutron scattering. *Proc. Natl Acad. Sci. USA*, **95**, 2267–2272.
42. Konarev, P. V., Volkov, V. V., Sokolova, A. V., Koch, M. H. J. & Svergun, D. I. (2003). PRIMUS: a Windows PC-based system for small-angle scattering data analysis. *J. Appl. Crystallog.* **36**, 1277–1282.
43. Crane, F. L., Glenn, J. L. & Green, D. E. (1956). Studies on the electron transfer system. The electron transfer particle. *Biochim. Biophys. Acta*, **22**, 475–48146.

Edited by R. Huber

(Received 3 May 2004; received in revised form 12 August 2004; accepted 25 August 2004)